





## Open Archive TOULOUSE Archive Ouverte (OATAO)

OATAO is an open access repository that collects the work of Toulouse researchers and makes it freely available over the web where possible.

This is an author-deposited version published in : <http://oatao.univ-toulouse.fr/>  
Eprints ID : 19836

**To link to this article** : DOI : 10.1016/j.surfcoat.2017.06.077  
URL : <http://dx.doi.org/10.1016/j.surfcoat.2017.06.077>

**To cite this version** : Michau, Alexandre  and Maury, Francis  and Schuster, F. and Boichot, R. and Pons, M. and Monsifrot, E. *Chromium carbide growth at low temperature by a highly efficient DLI-MOCVD process in effluent recycling mode.* (2017) *Surface and Coatings Technology*, vol. 332. pp. 96-104. ISSN 0257-8972

Any correspondence concerning this service should be sent to the repository administrator: [staff-oatao@listes-diff.inp-toulouse.fr](mailto:staff-oatao@listes-diff.inp-toulouse.fr)

# Chromium carbide growth at low temperature by a highly efficient DLI-MOCVD process in effluent recycling mode

A. Michau<sup>a</sup>, F. Maury<sup>a,\*</sup>, F. Schuster<sup>b</sup>, R. Boichot<sup>c</sup>, M. Pons<sup>c</sup>, E. Monsifrot<sup>d</sup>

<sup>a</sup> CIRIMAT, CNRS/INPT/UPS, 4 allée E. Monso, 31030 Toulouse cedex 4, France

<sup>b</sup> CEA Saclay, DFP/DPg, 91191 Gif Sur Yvette, France

<sup>c</sup> SIMAP, University Grenoble Alpes, CNRS, 38000 Grenoble, France

<sup>d</sup> DEPHIS, 74 rue Armand Japy, 25460 Etupes, France

---

## Keywords:

Chromium carbide  
Carbide coatings  
Hard coatings  
Recycling  
MOCVD process  
Bis(arene)chromium

---

The effect of direct recycling of effluents on the quality of Cr<sub>x</sub>C<sub>y</sub> coatings grown by MOCVD using direct liquid injection (DLI) of bis(ethylbenzene)chromium(0) in toluene was investigated. The results are compared with those obtained using non-recycled solutions of precursor. Both types of coatings exhibit the same features. They are amorphous in the temperature range 673–823 K. They exhibit a dense and glassy-like microstructure and a high hardness (> 23 GPa). Analyses at the nanoscale revealed a nanocomposite microstructure consisting of free-C domains embedded in an amorphous Cr<sub>7</sub>C<sub>3</sub> matrix characterized by strong interfaces and leading to an overall composition slightly higher than Cr<sub>7</sub>C<sub>3</sub>. The stiffness and strength of these interfaces are mainly due to at least two types of chemical bonds between Cr atoms and free-C: (i) Cr intercalation between graphene sheets and (ii) hexahapto η<sup>6</sup>-Cr bonding on the external graphene sheets of the free-C domains. The density of these interactions was found increasing by decreasing the concentration of the injected solution, as this occurred using a recycled solution. As a result, “recycled” coatings exhibit a higher nanohardness (29 GPa) than “new” coatings (23 GPa). This work demonstrates that using bis(arene)M(0) precursors, direct recycling of effluents is an efficient route to improve the conversion yield of DLI-MOCVD process making it cost-effective and competitive to produce protective carbide coatings of transition metals which share the same metal zero chemistry.

---

## 1. Introduction

For a better control of production cost of manufactured objects that comprise CVD coatings, the economic performance of deposition processes is an important need. The increasing use of metalorganic precursors is a way to reduce the cost of large-scale CVD process because this greatly lowers the deposition temperatures leading to substantial energy savings. This is evidenced for instance by the growth of metallic Cr at 673 K by DLI-MOCVD [1] in comparison with the industrial chromizing method of pack cementation which operates at about 1273 K.

A way to reduce the cost of CVD products is to repair the coating or to recycle the substrate. Indeed, though the coating and the substrate generally form strong and inseparable pairs there are examples where the substrate can be separated and recycled in CVD process to reduce the production cost. For instance in diamond coated cutting tools the worn coating was removed to apply a new one by the same CVD process [2] and, in the graphene CVD synthesis the Cu substrate used as catalyst

was recycled after delamination because it is an expensive substrate [3].

Another way to improve economic performance of CVD is to implement the recycling of effluents. Recycling in CVD processes is only mentioned in a basic book on the technique although it is important for applications [4]. When expensive molecular precursors are used, as for deposition of precious metals, the by-products are collected at the exit of the CVD reactor then leading recyclers and traders develop in parallel complex effluent treatments either to refine and reuse the collected precursor or to transform by-products and reuse pure metal [5]. This approach is also applied in high volume CVD production facilities. For instance a hydrogen recycle system was proposed recently for CVD of poly-Si [6]; in this case it is the carrier gas which is recycled. Also in the growth of Si for solar cells the exhaust gases (H<sub>2</sub>, HCl, chlorosilanes) were collected, separated and recycled [7]. Generally these strategies reduce the production cost but they did not act directly on the CVD process itself since the precursor is not directly recycled in a loop.

One of the advantages of CVD processes is the deposition of uniform

---

\* Corresponding author.

E-mail addresses: francis.maury@ensiacet.fr (F. Maury), frederic.schuster@cea.fr (F. Schuster), raphael.boichot@phelma.grenoble-inp.fr (R. Boichot), eric.monsifrot@dephis.com (E. Monsifrot).

coatings on 3D components with a high conformal coverage. This is achieved when the process operates in the chemical kinetic regime, *i.e.* at low pressure and low temperature. However, under these particular conditions the conversion efficiency of reactants is low (typically < 30%). Consequently to develop large-scale CVD processes using expensive reactants recycling of precursor become necessary to achieve a high conversion yield. For instance in the CVD production of boron fibers the selective condensation of unconverted BCl<sub>3</sub> is reused directly in the growth process [4]. Also the gas mixture CH<sub>4</sub>/H<sub>2</sub> recycling for diamond growth was reported [8] and a closed gas recycling CVD process has been proposed for solar grade Si [9]. Furthermore it was shown that a recycle loop is very useful for the management of the axial coating thickness uniformity of poly-Si in a horizontal low pressure CVD reactor [10], in agreement with the fact that the regime of the reactor is close to a Continuous Stirred Tank Reactor as previously demonstrated [11]. In these few examples the precursor is a hydride or a halide.

Metalorganic precursors become very important CVD sources thanks to the diversity of their molecular structures which allows controlling their chemical, physical and thermal properties. This allows satisfying the stringent requirements for the CVD process, *e.g.* low deposition temperature, high quality of the coatings.... Direct recycling of effluent using metalorganic precursors was not reported because the growth occurs at lower temperature than in hydride and halide chemistry and, in this condition, the quality of the layer strongly depends on the metal source which motivates many studies on molecular precursors [4,12–14]. Furthermore, these compounds generally undergo complex decomposition mechanisms producing many unstable metal-containing by-products. Kinetics plays a major role and the growth occurs far from thermodynamic equilibrium. Examples of complexity of decomposition pathways of Cr precursors are reported in [4,14,15].

The bis(arene)M(0) precursors, where M is a transition metal in the oxidation state zero of the columns 5 and 6 are an important family of CVD precursors for low temperature deposition of carbides, nitrides and even metal coatings. This is supported by several works using these precursors on carbides of V [16], Nb [17], Ta [17], Cr [18–21], Mo [22] and W [22], nitrides of V [16] and Cr [23] and metal V [16] and Cr [24,25], as well as nanostructured multilayer Cr-based coatings [26].

Chromium carbides are of great interest as tribological coatings for the protection of steel and metallic alloy components owing to their good resistance to corrosion and wear and their high hardness and melting point. They are used in many fields such as transports (automobile, shipping, aeronautic), mechanical and chemical industries and tools [27,28].

Our greater knowledge of the growth mechanisms of Cr-based coatings [24,29], thermodynamic modeling without [29] and with direct liquid injection (DLI) to feed the reactor [30], the determination of a kinetic model and the simulation of the CVD process [31] led us to study the effect of direct recycling of effluents on the quality of chromium carbide (Cr<sub>x</sub>C<sub>y</sub>) coatings grown by DLICVD using bis(ethylbenzene)chromium(0) as representative of this family. The results are compared with those obtained using a non-recycled solution of precursor. Both types of coatings exhibit the same features (composition, structure, hardness), demonstrating that using this specific chemical system, direct recycling of effluents is an efficient route to improve the conversion yield of DLI-MOCVD process making it very competitive to develop industrial applications. The barely significant difference of hardness is commented and selection criteria for molecular precursors

are also discussed so that they can be implemented in CVD processes with recycling of effluent.

## 2. Experimental

### 2.1. Deposition process

The growth was carried out at low temperature by direct liquid injection of metalorganic precursors in a CVD reactor (namely DLI-MOCVD process). It is a horizontal, hot-wall, Pyrex tubular reactor (300 mm long and 24 mm in internal diameter) with an isothermal zone around 150 mm. Stainless steel (304 L) plates and Si(100) wafers passivated by an amorphous SiN<sub>x</sub> thin layer acting as a barrier were used as substrates. They were placed on a planar horizontal sample-holder in the isothermal zone. More details are reported elsewhere [31]. The total pressure was automatically monitored and kept constant at 6.7 kPa and deposition temperature was set at 723 K.

Commercial bis(ethylbenzene)chromium (BEBC) from Strem (CAS 12212-68-9) was used as chromium precursor. It is in fact a viscous liquid mixture of several bis(arene)chromium compounds with the general formula [(C<sub>2</sub>H<sub>5</sub>)<sub>x</sub>C<sub>6</sub>H<sub>6-x</sub>]<sub>2</sub>Cr where x = 0–4 and BEBC is the major constituent. A solution in anhydrous toluene (99.8%) from Sigma-Aldrich (CAS 108-88-3) was prepared under inert atmosphere with a concentration of 3 × 10<sup>-1</sup> mol·L<sup>-1</sup> (4 g of BEBC in 50 mL of toluene). This precursor solution was injected in a flash vaporization chamber heated at 473 K using a Kemstream pulsed injector device. A liquid flow rate of 1 mL·min<sup>-1</sup> was set by adjusting the injection parameters in the ranges: frequency 1–10 Hz and opening time 0.5–5 ms. Nitrogen was used as carrier gas with a 500 sccm mass flow rate and was heated at approximately 453 K before entering the flash vaporization chamber to prevent condensation.

In this paper, “new” coatings refer to coatings elaborated using a freshly prepared liquid solution of as-received precursor and solvent, while “recycled” coatings concern coatings deposited using directly a recycled liquid solution of precursor, by-products and solvent. The same experimental parameters were used for new and recycled coatings: temperatures, pressure, injection parameters, carrier gas flow rate (the deposition time was about 1 h to inject about 160 mL of solution). The only difference was that the precursor concentration of the recycled solution was significantly lower due to consumption during previous runs. As a result, the growth rate in recycling mode was significantly lower. No attempt was made to change the deposition parameters in order to compare the characteristics of the coatings under identical growth conditions. The main CVD conditions are reported in Table 1.

The recycling mode investigated at this stage was based on an open-loop. This means gaseous by-products going out of the CVD reactor were forced to pass through a liquid nitrogen trap. Thus undecomposed molecules of BEBC and solvent were condensed in a tank with the reactions by-products (except light hydrocarbons as C<sub>2</sub> species whose trapping is not effective because of their high volatility). After returning to room temperature, a homogenous “daughter” liquid solution was obtained and stored in a pressurized tank under argon before further use. Several CVD runs were required to recover a sufficient amount of “daughter” solution for a recycled run. For example, we succeeded in obtaining a 1.5 μm thick coating with a recycled solution originating from two “new” deposition experiments which had each produced a 5 μm thick coating.

Each trapped solution could also be analyzed, for instance by UV

**Table 1**

Experimental DLICVD conditions of new Cr<sub>x</sub>C<sub>y</sub> coatings. The growth conditions in recycling mode are the same except that the BEBC solution injected resulting from cryogenic trapping during previous CVD runs had a lower concentration.

T (K)	P (kPa)	BEBC in toluene (mol/L)	BEBC gas flow rate (sccm)	Toluene gas flow rate (sccm)	N <sub>2</sub> gas flow (sccm)	Frequency (Hz)	Opening time (ms)
723	6.7	0.3	9	216	500	1–10	0.5–5

spectrophotometry to determine its precursor concentration. Indeed, BEBC exhibits a characteristic absorption band around 315 nm that could be used to measure the concentration according to the Beer-Lambert law (Supplementary material, Fig. S1). Also, as an improvement of the process, a closed-loop recycling system could also be installed and automated (currently in progress).

## 2.2. Coating characterization

The surface morphology and cross sections of coatings were characterized by scanning electron microscopy (SEM; Leo-435VP), and by electron probe micro-analysis (EPMA; Cameca SXFive) for the chemical composition. The crystalline structure was investigated at room temperature and ambient atmosphere by X-ray diffraction (XRD) in  $2\theta$  range [8–105°] using a Bruker D8-2 diffractometer equipped with a graphite monochromator (Bragg-Brentano configuration; Cu  $K_\alpha$  radiation). The microstructure of the coatings was also studied by transmission electron microscopy (TEM; Jeol JEM 2100 equipped with a 200 kV FEG, and a Bruker AXS Quantax EDS analyzer). For TEM observations, the samples were cut and thinned perpendicular to the surface by mechanical polishing, then prepared by a dimpling technique and thinned using a precision ion polishing system (PIPS, Gatan). By this method, the electron transparent area that can be observed is a cross section including the coating and the interface with the substrate.

The chemical environment of each element of the coating was investigated by X-ray photoelectron spectroscopy (XPS; Thermo Scientific K-Alpha) equipped with a monochromatic Al X-ray source and a low energy  $Ar^+$  gun (1 keV) for surface cleaning and depth profile analysis. Raman spectroscopy (Horiba Jobin Yvon LabRAM HR 800 with a 532 nm laser) was also used to analyze chemical bonding, in particular C–C bonds.

Hardness and Young's modulus were determined by nanoindentation using a Nano Scratch Tester (CSM Instruments). The loading/unloading cycle was respectively from 0 to 30 mN at 60  $mN \cdot min^{-1}$ , a pause of 30 s, then from 30 to 0 mN at 60  $mN \cdot min^{-1}$ . With this cycle the indenter penetration depth was lower than 1/10 of the coating thickness. For the thickest coatings, Vickers hardness was also measured using a BUEHLER OmniMet 2100 tester.

## 3. Results

### 3.1. General appearance and morphology

New and recycled coatings grown in the conditions reported in Table 1 exhibit the same glassy and dense microstructure, typical of an amorphous material. Interestingly, no grain boundary is observed by SEM, even at higher magnification than in Fig. 1, and it will be confirmed by TEM analysis in the Section 3.3. They have a metallic glossy appearance and a mirror-like surface morphology. Surface roughness of  $Cr_xC_y$  coatings on Si substrates measured by AFM gave similar values

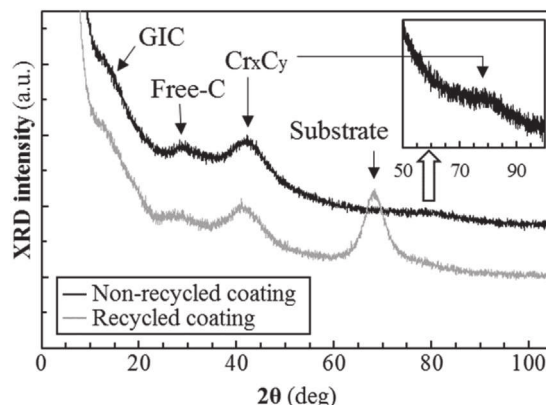


Fig. 2. Typical XRD pattern of a “new”  $Cr_xC_y$  coating grown by DLI-MOCVD with a new solution of BEBC in toluene (black) compared to that of a “recycled” coating (grey) grown in the same conditions.

for new and recycled coatings, typically  $rms = 18 \pm 2$  nm. Both types of coatings exhibit a very good conformal coverage on substrates with high surface roughness and on non-planar surfaces (edges, trenches...; not shown here). This is a great advantage of low pressure DLI-MOCVD which combines both a high diffusivity of gaseous reactants and decomposition at low temperature leading to a growth in the reaction-controlled regime. The only difference at this stage is the growth rate: recycled coatings were deposited with a lower growth rate than new coatings because of the lower precursor concentration of the recycled solution. Of course, this can be adjusted later.

### 3.2. Structure

A typical XRD pattern of a new coating 3.4  $\mu m$  thick grown at 723 K on Si substrate is presented and compared to a recycled coating in Fig. 2. In both cases, there is no evidence of diffraction peaks of polycrystalline phases. The pattern of the new coating is characteristic of an amorphous material with 4 weak and broad bumps, around  $2\theta = 13.8^\circ$ ,  $28.6^\circ$ ,  $42.5^\circ$  and  $79.0^\circ$  (better seen in the inset zoom). No difference was found for the recycled coating, except that due to its lower thickness, a broad peak originating from the substrate (amorphous  $SiN_x$  barrier layer) is observed at about  $69^\circ$  and the small bump at  $79^\circ$  is not as well marked.

The last two bumps from the coating at  $42.5^\circ$  and  $79.0^\circ$  corresponds to amorphous chromium carbides such as  $Cr_7C_3$  (JCPDS 00-036-1482) and  $Cr_3C_2$  (JCPDS 35-804) which both exhibits their main diffraction peaks in these two angular ranges. The FWHM of the most intense bump at  $42.5^\circ$  gives an average size of coherent domains close to 1 nm using Scherrer's formula, confirming the amorphous character of this carbide phase.

In carbon-containing materials the presence of graphite crystallites

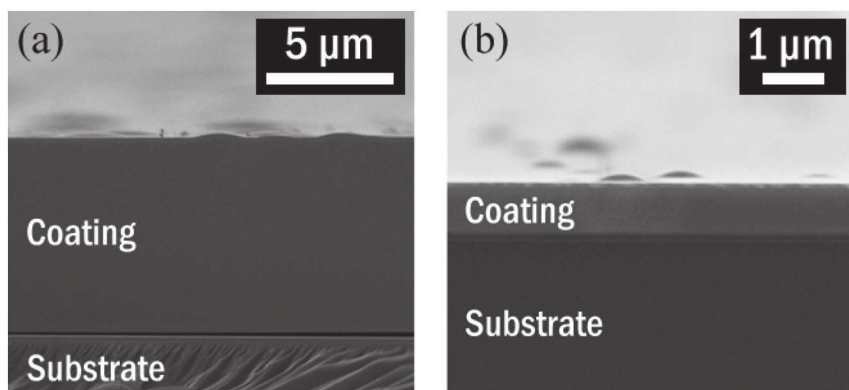


Fig. 1. Cross section of  $Cr_xC_y$  coatings grown at 723 K and 6.7 kPa on Si substrates using (a) a new BEBC solution in toluene and (b) a recycled solution. The lower thickness in (b) originates from the lower concentration of the recycled solution.

**Table 2**

Atomic composition of coatings grown with a new and recycled solution (EPMA data).

	Cr (at.%)	C (at.%)	O (at.%)
New Cr <sub>x</sub> C <sub>y</sub>	63.6 ± 1.7	33.1 ± 1.7	3.3 ± 2.0
Recycled Cr <sub>x</sub> C <sub>y</sub>	64.2 ± 0.2	30.6 ± 0.2	5.2 ± 0.2

is evidenced by the diffraction of the (002) plane expected at  $2\theta = 26.6^\circ$  in well crystallized graphite. However, disorder in hexagonal graphite structure (*e.g.* inside and between basal planes, stacking order between the graphene sheets, slipping out of alignment, folding...) leads to broadening and shifting of this peak. For instance pyrolytic carbon can exhibit a more or less disordered turbostratic or graphitic structure. Consequently the bump at  $28.6^\circ$  is assigned to pyrolytic carbon nanoparticles, namely free-C.

The first bump at  $2\theta = 13.8^\circ$  is not related to amorphous chromium carbides or to free-C. At this small angle (large interplanar spacing), this could be a compound with a lamellar structure derived from graphite, such as graphite oxide (GO). Indeed it has been reported that GO (001) plane diffracted from  $2\theta = 2$  to  $12^\circ$  depending on the presence of oxygen-containing groups [32]. However, the oxygen content of our coatings is lower than 5 at.% (Table 2), which is too low to support this hypothesis. Therefore the first bump at  $13.8^\circ$  was assigned to another derivative from graphite: the intercalation of Cr atoms between two graphene sheets as in graphite intercalation compound (GIC). Recently there are several reports dealing with the interactions between Cr and different forms of carbon, including graphene, nanotubes and fullerenes. For instance, a structural feature of the functionalization of graphene surface is the grafting of Cr which recreates locally the same type of bonding than in bis(arene)chromium, *i.e.* with an  $\eta^6$ -bonding to the aromatic cycles [33,34]. On the other hand, in sandwich graphene-Cr-graphene nanostructures, the representative distance of an ordered staking is twice the spacing between two consecutive graphene sheets, *i.e.* 6.556 Å, because Cr cannot be intercalated between two consecutive interlayer spaces as described in [33,34]. This corresponds to a diffraction angle  $2\theta = 13.5^\circ$  considering the (001) plane, which is very close to our  $13.8^\circ$  experimental value (Fig. 2).

### 3.3. Microstructure

From approximately the same magnification as in SEM images (Fig. 1) and to larger values up to high resolution, TEM images showed the same glassy microstructure for Cr<sub>x</sub>C<sub>y</sub> coatings, as it can be seen on Fig. 3a. Again no significant difference was found for recycled coatings. A high resolution TEM analysis (Supplementary material, Fig. S2) has revealed a dense and very finely granular structure with homogeneous and monodisperse distribution of contrasted domains. The average size of these domains is of the order of magnitude of 1 nm, in good

agreement with the value found by XRD.

The selected area electron diffraction pattern of the micrograph shown in Fig. 3a revealed two diffuse rings (Fig. 3b) as for high resolution TEM analysis in Fig. S2. They are centered on interplanar distances 2.097 Å and 1.223 Å. In accordance with the Bragg relation, they correspond to theoretical XRD diffraction angles at  $2\theta = 43.1^\circ$  and  $78.1^\circ$ . Therefore, the inner and outer rings on TEM diffraction patterns correspond to the first and the second Cr<sub>x</sub>C<sub>y</sub> bumps on XRD pattern found at  $2\theta = 43.5^\circ$  and  $79.0^\circ$ , respectively (Fig. 2). This is supported by the fact that both crystalline Cr<sub>7</sub>C<sub>3</sub> and Cr<sub>3</sub>C<sub>2</sub> phases show their strongest XRD contributions in the  $2\theta$  range  $39\text{--}44^\circ$  and they also exhibit a second bunch of peaks with a lower intensity around  $2\theta = 80^\circ$ . The two bumps on XRD pattern at  $2\theta = 13.8^\circ$  and  $28.6^\circ$  assigned to GIC and free-C respectively, were not seen on TEM diffraction pattern likely because they were too weak and diffuse for this technique.

### 3.4. Chemical composition

Atomic composition determined by EPMA of new and recycled coatings is reported in Table 2. No significant difference is observed between both coatings; it is typically Cr<sub>0.64</sub>C<sub>0.33</sub>O<sub>0.03</sub>. The level of oxygen contamination is slightly higher in recycled coatings but it does not exceed about 5 at.%. This was attributed to the handling of the recycled solution that was stored in a pressurized tank. Although handled under Ar atmosphere this container had to be opened and closed several times in order to recover enough solution after several deposition experiments for a further use in a recycling CVD run. By neglecting traces of oxygen, the total carbon content of these carbide coatings (C:Cr =  $0.50 \pm 0.02$ ) is intermediate between Cr<sub>7</sub>C<sub>3</sub> (C:Cr = 0.43) and Cr<sub>3</sub>C<sub>2</sub> (C:Cr = 0.67) but it is closer to Cr<sub>7</sub>C<sub>3</sub>. The overall atomic composition is consistent with a nanocomposite structure consisting of an amorphous carbide matrix *a*-Cr<sub>x</sub>C<sub>y</sub> and free-C, as supposed from XRD and TEM results, and the ratio *y*:*x* in the matrix is lower than 0.50, *i.e.* even closer to the Cr<sub>7</sub>C<sub>3</sub> stoichiometry.

XPS analyses did not reveal significant difference between both types of coatings, except a higher contribution of oxygen bonded to Cr for recycled coatings, in agreement with EPMA data. As-deposited samples exhibit Cr 2p<sub>3/2</sub> peaks characteristic of Cr(III) oxide (575.8 eV) and Cr–OH (576.8 eV), O 1s peaks were assigned to Cr<sub>2</sub>O<sub>3</sub> (530.8 eV) and C–O/OH (532.0 eV), and C 1s core level was characteristic to adventitious carbon with the components C–C/C–H at 284.8 eV and O–C=O at 288.0 eV. A depth profile analysis of C 1s showed that Ar<sup>+</sup> ion etching of the sample for about a minute at 1 keV removes readily the surface contamination without significant secondary effect of sputtering (Fig. 4a). The C 1s region of as-deposited sample shows the main features of adventitious carbon with the C–C/C–H and O–C=O components (Fig. 4b). After removal of the contamination layer by ion etching for 220 s the C 1s peak reveals two forms of carbon present in the coating: the carbide (282.8 eV) and the free-C (~284 eV) as

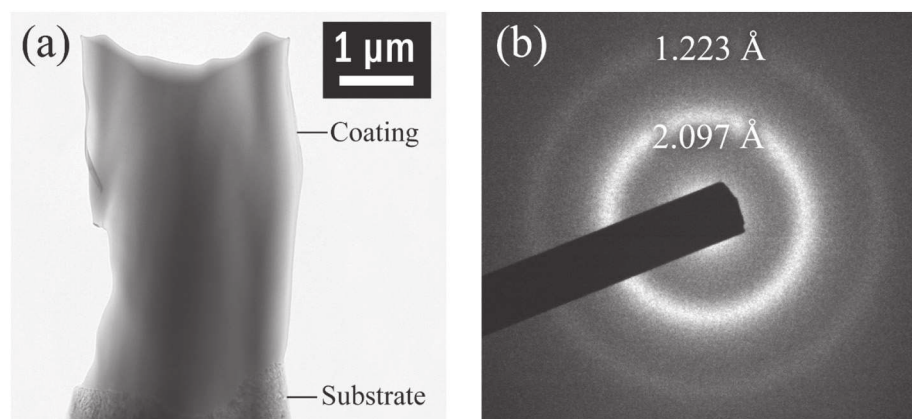


Fig. 3. (a) TEM micrograph of a new Cr<sub>x</sub>C<sub>y</sub> coating observed in cross section; (b) corresponding selected area electron diffraction showing two diffuse rings of the amorphous carbide phase.

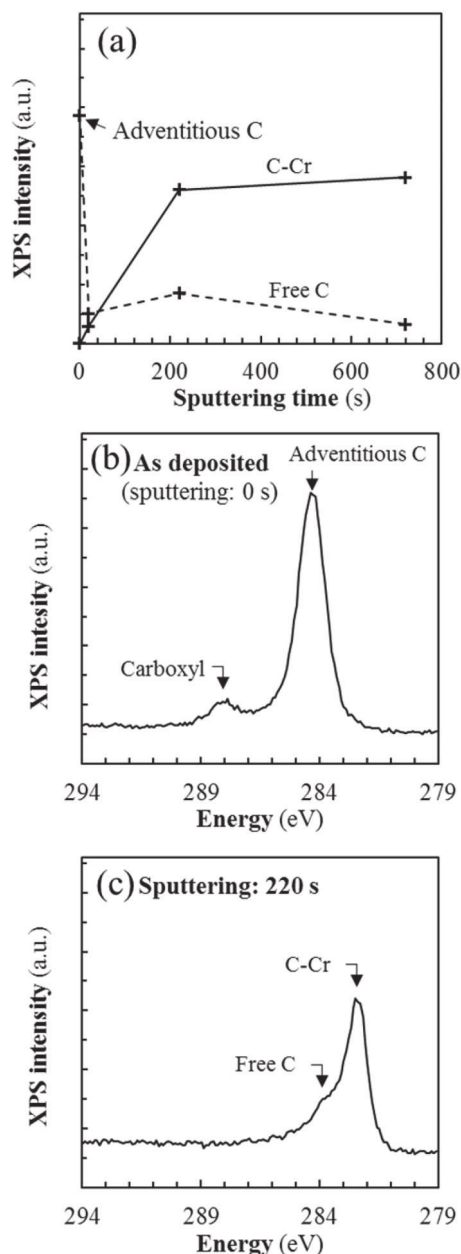


Fig. 4. XPS analysis of a new  $\text{Cr}_x\text{C}_y$  coating: (a) depth profile of C 1s components, (b) C 1s spectra of as-received sample (0 s ion etching time) and (c) C 1s spectra after 220 s ion etching time.

minority component (Fig. 4c). After the surface cleaning by ion etching, the O 1s intensity is significantly decreased and only one component is found at 530.8 eV (Cr–O). Regarding Cr  $2p_{3/2}$  region, the oxygenated components have almost disappeared and the peak is shifted to 574.0 eV as for Cr metal or carbide (Cr–C bonds). This XPS analysis confirms the presence of free-C and a carbidic form in the coatings as observed by XRD. After *in situ* surface cleaning the atomic composition of the surface analyzed by XPS is  $\text{Cr}_{0.57}\text{C}_{0.33}\text{O}_{0.10}$  that is in good agreement with EPMA data (Table 2). From the relative intensity of the two components of C 1s peak of Fig. 4c the proportion of free-C to the total-C is approximately 20%. On the other hand, considering the EPMA composition  $\text{Cr}_{0.64}\text{C}_{0.33}\text{O}_{0.03}$  (Table 2) as a representative formula and neglecting oxygen content, comparison with the stoichiometric  $\text{Cr}_7\text{C}_3$  phase reveals a carbon excess as free-C of 18 at.%. These two values of relative content of free-C determined by XPS and EPMA are in good agreement and confirm the presence of free-C nanostructures identified

in XRD. Due to the presence of free-C, it is confirmed that the matrix  $\alpha\text{-Cr}_x\text{C}_y$  has the composition  $\alpha\text{-Cr}_7\text{C}_3$ .

The coatings being of metallic nature, Raman spectra should not be *a priori* readily informative. Raman signal originates only from surface oxides and carbon components; no response was expected from a metallic matrix. Fig. 5 compares the Raman spectra of a new and a recycled coating for the 200 to 1800  $\text{cm}^{-1}$  spectral range. Overall, the large width of the bands reveals the absence of long-range order, either because of the amorphous character of the phases or because of defects. At first glance the spectra appear very different but they are both constituted of two zones with different intensities. The bands in the first zone (200–1000  $\text{cm}^{-1}$ ) are essentially due to chromium oxides on the surface of the sample [35–37] while the bands in the second zone (1000–1800  $\text{cm}^{-1}$ ) are characteristic of carbon in different environments [38]. In comparison with the new coating (Fig. 5a), the higher intensity of the bands in the first zone for the recycled coating is consistent with a substantially greater oxidation (Fig. 5b), in good agreement with EPMA and XPS analyses.

Spectra deconvolution on Fig. 5c and d reveals the D band at 1340  $\text{cm}^{-1}$  and the G band at 1570  $\text{cm}^{-1}$  which are representative of C–C bonds [38]. G stands for graphite and D for disorder in graphitic structures. The bands at 1225 and 1455  $\text{cm}^{-1}$  were assigned to *trans*-polyacetylene, a strong polymeric chain  $-(\text{C}_2\text{H}_2)_n-$  where carbon adopts  $\text{sp}^2$  configuration [38]. Because of overlaps with the bands of *trans*-polyacetylene, the presence of C  $\text{sp}^3$  cannot be ruled out since it is expected at 1180 and 1332  $\text{cm}^{-1}$  in nanocrystalline and cubic diamond respectively, and at 1500  $\text{cm}^{-1}$  in DLC (disordered  $\text{sp}^3$  hybridization) [39].

In carbon materials, correlations were established between the development of the disorder from  $\text{sp}^2$  structural model (graphite) to  $\text{sp}^3$  (diamond) and the variation of the intensity ratio  $I(D)/I(G)$  as well as the FWHM and the position of the G band [38–40]. Fig. 5 shows that the intensity ratio  $I(D)/I(G)$  significantly increases from new coatings ( $\sim 0.6$ ) to recycled coatings ( $\sim 1.2$ ), suggesting that the disorder within graphitic nanostructures is higher for the recycled sample. The fact that the relative intensity of the bands at 1220 and 1460  $\text{cm}^{-1}$  assigned to *trans*-polyacetylene and possibly to C  $\text{sp}^3$  does not change from a new coating to a recycled one suggests that the evolution of the disorder cannot be interpreted in terms of C  $\text{sp}^3$  proportion. As a result, it is more appropriate to consider interactions between Cr and free-C as structural defects (both in-plane and between graphene sheets) that cause increasing disorder when their number increases.

The average size of graphitic nanoparticles in the basal plane determined from the FWHM of the G band, namely  $L_a$  [38], remains constant at around 35 nm for both new and recycled coatings. On the other hand, a disorder measurement  $L_D$  can be determined from the intensity ratio  $I(D)/I(G)$ ; it represents the average distance between two point defects in graphene planes [40]. As suggested above, Cr grafting on graphene sheet can be considered as a defect which induces disorder. Thus,  $L_D$  can be considered as the average distance between two grafted Cr and it was found decreasing from 15.5 to 6.2 nm for new and recycled coatings respectively. This means that despite an identical overall atomic composition, recycled coatings exhibit a higher defect density, as interactions at the free-C/ $\alpha\text{-Cr}_7\text{C}_3$  interfaces, *e.g.* both as hexahapto- $\eta^6$ -Cr grafting on external graphene sheets and Cr intercalation between graphene layers.

### 3.5. Hardness

For the thickest  $\text{Cr}_x\text{C}_y$  new coatings ( $\sim 5 \mu\text{m}$ ), Vickers hardness around 2300 HV was measured which is quite high for CVD chromium carbide coatings. Values in the range 700–1600 HV were previously reported for polycrystalline MOCVD chromium carbides coatings [41,42] while electrodeposited  $\text{Cr}_x\text{C}_y$  coatings did not exceed 1300 HV<sub>100</sub> [43,44] and electroplating hard Cr is lower than 1200 HV [45,46]. Only PVD processes manage to reach even higher hardness,

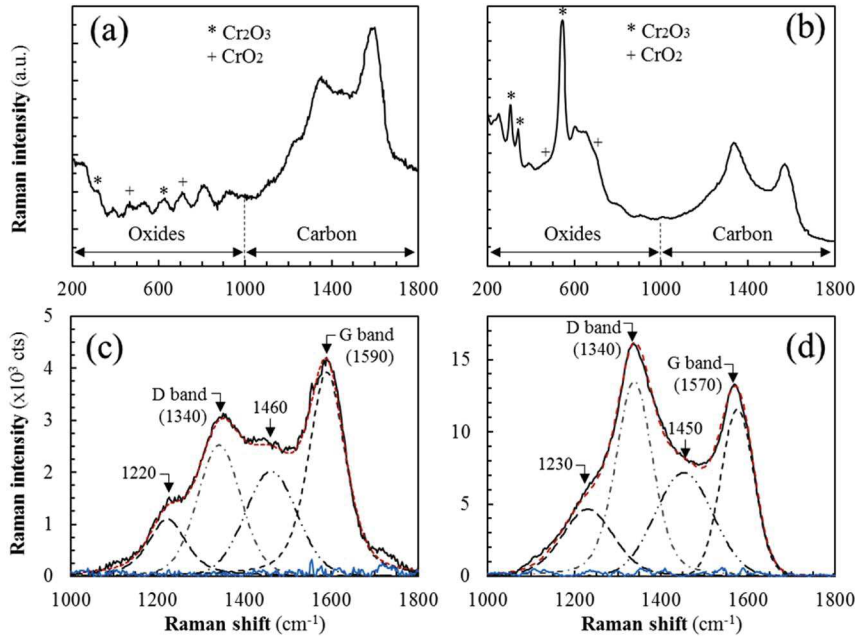


Fig. 5. Raman spectra of  $\text{Cr}_x\text{C}_y$  coatings grown on a Si substrate with a new BEBC solution (a) (c), and a recycled one (b) (d): spectral range 200–1800  $\text{cm}^{-1}$  (a) (b), and the C region (c) (d). The proposed deconvolution of the C bands is commented in the text.

from 2000 to 3000 HV [47–49].

For the thinnest  $\text{Cr}_x\text{C}_y$  coatings ( $\leq 3.5 \mu\text{m}$ ), hardness was determined by nanoindentation on five samples corresponding to three new and two recycled coatings. The values of hardness (H) and Young's modulus (E) reported in Table 3 are the average of at least ten successful indentations per sample. Considering standard deviations of measurements, new and recycled coatings have substantially comparable H and E values. Nanoindentation measurements confirmed Vickers hardness tests. With values in the range 23–29 GPa for coatings on 304 L thicker than 1  $\mu\text{m}$ , both types of coatings exhibit nanoindentation hardness as high as those of  $\text{Cr}_x\text{C}_y$  coatings deposited by PVD, e.g. 24.2 GPa [50], 22 GPa [51] and 21 GPa [52], as well as MOCVD, 25 GPa [53]. It is noteworthy that our coatings are amorphous, whereas those in the cited references were polycrystalline.

While there is no difference on the Young's modulus between new and recycled coatings (285 and 295 GPa, respectively), the nanoindentation hardness of recycled coatings could be considered slightly higher (29 GPa) than that of new coatings (23 GPa), despite the standard deviations. This will be discussed in the next section. The ratio  $H^3/E^2$  is often referred as a durability criteria; it is proportional to the contact loads needed to induce plasticity and consequently it characterizes the resistance to induce plastic deformation [54,55]. Comparison of both types of coatings revealed a better behavior of recycled coatings as a result of their higher hardness, the ratio  $H^3/E^2$  being increased almost 3-fold.

#### 4. Discussion

Chromium carbide coatings were successfully deposited using directly recycled solutions in the same DLI-MOCVD conditions as using new bis(ethylbenzene)chromium solutions. The growth rate in effluent recycling mode was found lower (around 0.5–1  $\mu\text{m}\cdot\text{h}^{-1}$  instead of 5–10  $\mu\text{m}\cdot\text{h}^{-1}$ ) essentially because the recycled BEBC solution in toluene

Table 3  
Nanoindentation results for new and recycled coatings deposited on 304 L stainless steel substrate.

Coating	Thickness ( $\mu\text{m}$ )	H (GPa)	E (GPa)	$H^3/E^2$ (GPa)
New $\text{Cr}_x\text{C}_y$	3.5	23 $\pm$ 2	285 $\pm$ 20	1.4 $\times 10^{-1}$
Recycled $\text{Cr}_x\text{C}_y$	1.0	29 $\pm$ 4	295 $\pm$ 40	3.9 $\times 10^{-1}$

was less concentrated due to consumption in previous runs. Chemical and structural characterizations of both types of coatings did not reveal significant differences. The coatings exhibit a smooth surface morphology, a dense and glassy-like microstructure and an amorphous structure (XRD and TEM analyses). The overall atomic composition was found to be  $\text{Cr}_{0.64}\text{C}_{0.33}\text{O}_{0.03}$  (Table 2). Interestingly, both coatings exhibit a high conformal coverage on non-planar surfaces at relatively low deposition temperature (723 K).

##### 4.1. A high hardness

This section discusses on the one hand the high values of hardness of the coatings whatever the precursor solution injected (new or recycled) and, on the other hand, on the difference of nanohardness between recycled and new coatings, assuming therefore that the difference is significant enough.

Both Vickers hardness (2300 HV) and nanoindentation hardness (23–29 GPa) have revealed high values, at the level of those previously reported for PVD  $\text{Cr}_x\text{C}_y$  coatings [50–52]. A great advantage of DLI-MOCVD  $\text{Cr}_x\text{C}_y$  coatings is that they are amorphous, without grain boundaries, while those deposited by other processes are polycrystalline. It is generally reported that crystalline chromium carbides coatings grown by PVD [51], cathodic arc evaporation [51] and electrodeposition [43] are harder than amorphous ones. Interestingly the hardness of our amorphous coatings is already at the level of these polycrystalline  $\text{Cr}_x\text{C}_y$  coatings. Consequently, their amorphous structure cannot explain their high hardness. We are aware that  $\text{Cr}_3\text{C}_2$  is the hardest phase of Cr–C system and therefore its presence, even in the amorphous state, should significantly increase the hardness. However, we have shown that the matrix of our coatings has the stoichiometry  $a\text{-Cr}_7\text{C}_3$ . Also it is known that for nanocrystalline  $\text{Cr}_x\text{C}_y$  coatings, the nanohardness increased by decreasing the average grain size [44]. Without evidence for nanocrystalline structure this claim does not hold for our coatings. It was also reported that a high hardness was achieved for high Cr contents [50], or that stoichiometric Cr–C phases must be privileged, meaning a C excess must be avoided [52]. We will discuss below that in our case a C excess, compared to  $\text{Cr}_7\text{C}_3$  stoichiometry, on the contrary plays a key role.

Among the factors that influence the hardness of coatings, residual stresses are probably the most important [56]. The influence of other factors as coating thickness, growth conditions, micro- and

nanostructure has been reported but they act both on the stresses and the hardness, and so their effect is difficult to decouple.

For two new coatings 3.5 and 35.0  $\mu\text{m}$  thick the nanohardness and Young modulus were found constant at  $23.6 \pm 2.0$  GPa and approximately 293 GPa, respectively. This means the nanohardness is independent of the thickness for values higher than 3.5  $\mu\text{m}$ . At this stage no data is available for thinner coatings to comment on the possible influence of thicknesses lower than 3.5  $\mu\text{m}$ . It is noteworthy that our experimental value of the Young's modulus is in good agreement with the  $\text{Cr}_7\text{C}_3$  theoretical value of 302 GPa [57].

In coating-substrate systems prepared by CVD, residual stresses ( $\sigma_r$ ) originate from the sum of thermal stresses ( $\sigma_t$ ) induced by the mismatch of thermal expansion between the coating and the substrate, and intrinsic stresses ( $\sigma_i$ ) induced by the growth mechanism. The residual stresses were determined for two "new" coatings (thickness  $t_f = 4.0$  and 6.0  $\mu\text{m}$ ) deposited on 304 L steel strip 0.5 mm thick ( $t_s$ ). As the ratio  $t_f/t_s$  (or  $E_f t_f/E_s t_s$ ) is  $\leq 1\%$  [58], the deformation of the substrate can be negligible. The  $E_i$ 's are the biaxial moduli ( $E_i/(1 - \nu_i)$ ),  $t_i$  the thicknesses,  $\nu_i$  the Poisson's ratio and the subscripts s and f respectively denotes the substrate and the film, which leads to  $E_f' = 363$  GPa and  $E_s' = 278$  GPa using  $\nu_{\text{CrC}} = 0.2$  and  $E_{\text{CrC}} = 290$  GPa (average data of  $\text{Cr}_7\text{C}_3$  and  $\text{Cr}_3\text{C}_2$ ). The Stoney's equation is applicable with an error which does not exceed 5%. From the measurement of the change of curvature before and after deposition, compressible residual stresses of  $-1.20$  and  $-1.25$  GPa were found for the 4.0 and 6.0  $\mu\text{m}$  thick coatings, respectively. Reliable data could not be obtained by this method for recycled coatings because they were too thin. Assuming a rigid substrate, the maximum thermal stress can be calculated according to the equation:

$$\sigma_i = E_f'(\alpha_f - \alpha_s)\Delta T.$$

where  $\Delta T$  is the variation of temperature and  $\alpha_i$  the thermal expansion coefficient ( $\alpha_s = 18.3 \times 10^{-6} \text{K}^{-1}$  and  $\alpha_f = 10.1 \times 10^{-6} \text{K}^{-1}$ ). For  $\Delta T = 430$  K, calculated thermal stresses are  $-1.32$  GPa. These values are generally found for ceramic coatings as TiN on stainless steel substrates [59]. These results are confirming the dominant contribution of thermal stresses to residual stresses.

The comparison of hardness of new ( $23 \pm 2$  GPa) and recycled ( $29 \pm 4$  GPa) coatings reveals a small but significant difference, taking into account the standard deviations, which raises the question: why should recycled coatings be harder? This could be discussed in terms of residual stresses but no data are available for recycled coatings. However, the residual stresses are largely dominated by thermal stress which has the same value for both coatings since they were deposited at the same temperature and their thickness was relatively close (3.5 and 1.0  $\mu\text{m}$ , respectively). Consequently this is likely not a major factor to explain the difference of hardness. One of the best ways to comment on this difference in hardness is to focus on the specific nanocomposite structure of these hard coatings since it is known that this influences the hardness.

#### 4.2. A specific amorphous nanocomposite structure

The morphology, microstructure and composition of new and recycled coatings are the same. Furthermore, XRD, XPS and Raman analyses gave evidence for an amorphous nanocomposite structure. The only significant differences between both types of coatings were found by Raman spectroscopy (Fig. 5).

Basically, the microstructure is composed of 2 phases with interfaces acting as strong interphases. The dominant phase is an amorphous carbide matrix with the  $\text{Cr}_7\text{C}_3$  stoichiometry (namely  $a\text{-Cr}_7\text{C}_3$ ). Nanometric free-C domains ( $L_a = 35$  nm in-plane correlation length) are embedded in this amorphous carbide matrix. They are related to pyrolytic C, which means they exhibit a disordered graphitic structure (turbostratic stacking) with likely some covalent bonding between graphene sheets *via* open cycles at the edges (generating C  $\text{sp}^3$  sites).

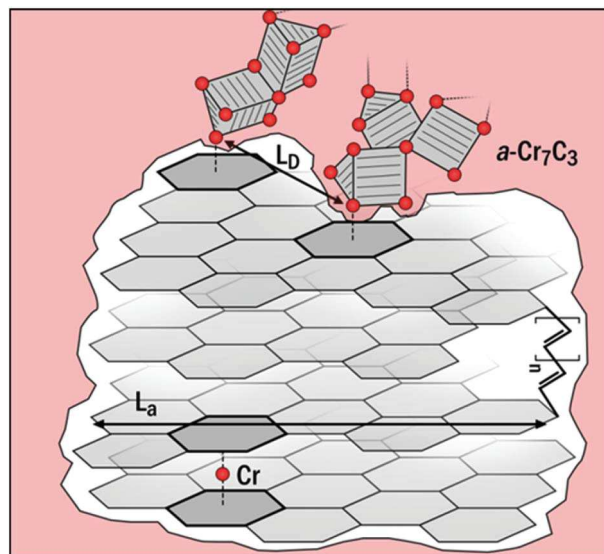


Fig. 6. Schematic representation of the amorphous and nanocomposite microstructure of  $\text{Cr}_x\text{C}_y$  coatings deposited by DLI-MOCVD showing the main structural features at the interface between free C nanostructures embedded in an amorphous  $\text{Cr}_7\text{C}_3$  matrix (Cr atoms are the red circles). The  $L_a$  and  $L_D$  distances shown are discussed in the text. (For interpretation of the references to color in this figure legend, the reader is referred to the web version of this article.)

Furthermore, some graphene sheets are also connected by *trans*-polyacetylene chains at the edges of these C domains. The relative amount of free-C does not exceed 20% of the total carbon (XPS and EPMA data). An important finding was to identify signatures by Raman and XRD revealing interactions between Cr and free-C. This particular nanostructure is shown schematically in Fig. 6. Due to their layered structure, the free-C domains exhibit two types of interfaces with the  $a\text{-Cr}_7\text{C}_3$  matrix: the one which is parallel to the graphene sheets (parallel interface) and that which is roughly perpendicular to the stacking of graphene planes (perpendicular interface). Cr atoms from the amorphous carbide matrix can be grafted on external graphene sheets as hexahapto  $\eta^6\text{-Cr}$  complexes of graphene [34]. These specific bonds are very similar to those in the BEBC precursor. They contribute to the strengthening of the parallel interfaces. Also, individual Cr atoms can be intercalated between consecutive graphene sheets as in graphite intercalation compounds as supported by XRD data (Fig. 2) [33,34]. All these Cr interactions can be considered as point defects in ideal graphene sheets. Despite a graphitic base structure, these interactions and interconnections between free-C and  $a\text{-Cr}_7\text{C}_3$ , through C  $\text{sp}^3$ , *trans*-polyacetylene and  $\eta^6\text{-Cr}$  bonding rigidify the free-C domains, strengthen the interfaces and consolidate a 3D structural network between the carbide matrix and free-C through strong interphases.

The defect density on the external graphene sheets of free-C nanostructures has been estimated from Raman data as the average distance  $L_D$  between two point defects in graphene sheet (Fig. 6). Interestingly  $L_D$  was found to decrease from 15.5 to 6.2 nm for new and recycled coatings, respectively, while the average size of graphene sheet given by in-plane correlation length  $L_a$  is constant (35 nm). This means the defect density, *i.e.* the density of interactions between the carbide matrix and free-C is significantly higher for recycled coatings than for the new ones. This trend suggests a correlation with the higher hardness of recycled coatings ( $29 \pm 4$  GPa) compared to the new coatings ( $23 \pm 2$  GPa). The nanohardness would increase with the density of chemical bonds both within graphene sheets of the free-C nanostructures and between these free-C domains and the amorphous carbide matrix.

Basically the growth mechanism is the same for "new" and "recycled" coatings. A simple chemical mechanism reduced to 4 limiting reactions (1 homogeneous, 3 heterogeneous) was proposed for kinetic



modeling and simulation of the process. It is based on site competition reactions [31]. The lower concentration of recycled BEBC solutions would induce a lower supersaturation of BEBC near the growing surface. As a result, this would favor a higher mobility of adsorbed chemical species or would influence adsorption competition and finally would facilitate locally the formation of chemical bonds both within the C domains (C sp<sup>3</sup>, *trans*-polyacetylene bridges) and at the parallel and perpendicular interfaces with the amorphous carbide matrix (Cr grafting and intercalation, respectively). Subsequently the nanostructure of the coating is overall strengthened and its nanohardness is increased.

Another hypothesis about strong interphases instead of sharp and weak interfaces, not supported here by experimental data, is to be aware that in the crystallographic structure of Cr<sub>7</sub>C<sub>3</sub> carbon atoms are in trigonal prisms connected in chains while it was reported that in amorphous Cr<sub>1-x</sub>C<sub>x</sub> for x > 33% carbon progressively filled octahedral interstitial sites as the C content increased, suggesting that C coexisted in both prismatic and octahedral sites [60]. It is reasonable to assume that at the interface *α*-Cr<sub>7</sub>C<sub>3</sub>/free-C a carbon enrichment of the carbide matrix is possible by the gradual occupation of both prismatic and octahedral sites. For instance in C-rich amorphous Cr<sub>x</sub>C<sub>y</sub> grown by PVD, C atoms were located in a mixture of prismatic and octahedral sites with a distribution depending on the total C content [61]. These polyhedral units are characterized by strong covalent Cr 3d-C 2p bonding. Locally, at the *α*-Cr<sub>7</sub>C<sub>3</sub>/free-C interface, the proportion of C atom filling octahedral sites probably depends on growth conditions. If the growth rate of the *α*-Cr<sub>7</sub>C<sub>3</sub> matrix is slow enough, for instance because the mole fraction of precursor is low, in a competitive pathway C can diffuse to fill octahedral sites and thus strengthen the interphase.

At this stage it is not reasonable to speculate more on the difference of hardness between “new” and “recycled” coatings because the difference is not so large and it must be confirmed by other experiments. However, it can be retained that both the density of interactions between the carbide matrix and free-C (grafting and intercalation of Cr), supported by experimental data, and the assumed gradual occupation of prismatic and octahedral sites of the carbide by the carbon generate strong interphases which influence the mechanical properties.

#### 4.3. Key points making recycling possible: selection of precursor

A barrier in the implementation of MOCVD recycling is that the decomposition of the metalorganic precursor is complex and often produces many by-products which, if recycled, significantly affect the composition and microstructure of the coatings. Consequently a tedious and expensive separation of the by-products is necessary to recover the precursor which has not reacted. The key is therefore to use metalorganic precursors whose decomposition mechanism is very simple, and which do not produce metalorganic by-products that could modify the growth mechanism.

This is the case of bis(arene)M(O) compounds where the metal M is in the zero valence state, as in the deposited metal or carbide coatings. This important family of precursors was used for low temperature MOCVD of carbides of V [16], Nb [17], Ta [17], Cr [18–21], Mo [22] and W [22]. In the deposition process the metal, and in particular Cr, stays in the zero valence state. For instance no hexavalent Cr(VI) compound is formed which entirely satisfies European regulation REACH or related rules. The ligands are stable aromatic molecules; they are readily released by selective bond breaking during the deposition process without undergoing significant pyrolysis [24,62]. It is then recommended in DLI-MOCVD to use solvent of the same family as the ligands (e.g. toluene for BEBC) to avoid uncontrolled side-reactions.

The main characteristics of the coatings are independent of the nature of the ligands as deduced from the use of Cr(C<sub>6</sub>H<sub>6</sub>)<sub>2</sub>, Cr(C<sub>6</sub>H<sub>5</sub><sup>*t*</sup>Pr)<sub>2</sub> and Cr(C<sub>6</sub>H<sub>5</sub>Et)<sub>2</sub> [19,20]. As a result, a mixture of different bis(arene)Cr precursors can be used as in [63,64] and in this work. Also the nature of the solvent is not very important provided that it is non-

reactive, thermally stable in the deposition temperature range, and therefore does not participate in the growth mechanism as found using toluene and cyclohexane [26,65].

The solution recovered in the cold trap at the exit of the CVD reactor contains undecomposed BEBC, toluene (solvent) and a mixture of organic by-products originating from the released ligands and the heterogeneous decomposition of a small part of them producing ethylbenzene, diethylbenzene, benzene, ethyltoluene, toluene [62] as well as lighter and non-aromatic hydrocarbons and hydrogen [24]. The lighter hydrocarbons and hydrogen are not efficiently trapped because of their high volatility. The organic by-products originating from the ligands are of the same family as the solvent. Consequently, the trapped solution that can be directly recycled contains unreacted BEBC and solvents constituted of a mixture of several aromatic hydrocarbons. The major difference with the new solution is that the BEBC concentration in the recycled solution is lower due to its consumption. Finally, direct recycling of all effluents can be implemented using this chemical system in a close-loop to reach a conversion rate of the precursor near 100% (currently in progress).

## 5. Conclusions

The impact of the high cost of metalorganic precursors on the economic viability of MOCVD can be overcome by maximizing the conversion yield. It was demonstrated that direct recycling of effluent is possible using appropriate bis(arene)Cr(0) precursors.

Chromium carbide coatings were deposited by DLI-MOCVD using either a new bis(ethylbenzene)chromium solution in toluene or a recycled solution recovered at the exit of the reactor. Chemical and structural characteristics of both types of coatings are very similar. They are amorphous with a composition slightly higher than Cr<sub>7</sub>C<sub>3</sub>. The nanohardness is particularly high with values in the range 23–29 GPa. This high hardness is essentially due to the nanocomposite microstructure, without grain boundary, and strong interphases between free-C domains embedded in an amorphous Cr<sub>7</sub>C<sub>3</sub> matrix. The slightly higher hardness of recycled coatings was assigned to a higher density of chemical bonds both within the C domains (C sp<sup>3</sup> and *trans*-polyacetylene bridges) and at the interfaces with the amorphous carbide matrix (Cr grafting and intercalation). A gradual filling of prismatic and octahedral C sites of the matrix also likely plays a role in strengthening the interphase.

It is a breakthrough for MOCVD because the process can be extended to metals of columns 5 and 6 for which the same M(0) chemistry can be implemented and the carbides also have many practical applications as protective metallurgical coatings. Recycling in a closed-loop is currently in progress to reach a conversion rate near 100% in a one-step CVD run.

## Acknowledgements

This work was supported by the Centre of Excellence of Multifunctional Architected Materials “CEMAM” [grant number AN-10-LABX-44-01]. We thank Sofiane Achache and Raphaël Laloo for their help in hardness measurements, Jerome Esvan and Olivier Marsan for their assistance in XPS and Raman spectroscopies.

## Appendix A. Supplementary data

Supplementary data to this article can be found online at <https://doi.org/10.1016/j.surfcoat.2017.06.077>.

## References

- [1] A. Michau, F. Maury, F. Schuster, R. Boichot, M. Pons, Evidence for a Cr metastable phase as a tracer in DLI-MOCVD chromium hard coatings usable in high temperature environment, *Appl. Surf. Sci.* 422 (2017) 198–206.

- [2] H. Liu, H. Hanyu, Y. Murakami, S. Kamiya, M. Saka, Recycling technique for CVD diamond coated cutting tools, *Surf. Coat. Technol.* 137 (2001) 246–248.
- [3] Y. Wang, Y. Zheng, X. Xu, E. Dubuisson, Q. Bao, J. Lu, K.P. Loh, Electrochemical delamination of CVD-grown graphene film: toward the recyclable use of copper catalyst, *ACS Nano* 5 (2011) 9927–9933.
- [4] W.S. Rees Jr., Introduction, in: W.S. Rees Jr. (Ed.), *CVD of Nonmetals*, Weinheim, VCH, 1996, pp. 1–35.
- [5] Recycling International, Japanese recycling process for ruthenium precursors, <http://www.recyclinginternational.com/recycling-news/3464/research-and-legislation/japan/japanese-recycling-process-ruthenium-precursors>, (2010), Accessed date: 17 January 2017.
- [6] V. Revankar, S. Lahoti, CVD-Siemens reactor process hydrogen recycle system. US20150107298 A1, (2015).
- [7] Poly plant project, off-gas recovery & recycling, <http://www.polyplantproject.com/offgasrecoveryrecycling.html>, (2010), Accessed date: 17 January 2017.
- [8] F.X. Lu, W.Z. Tang, G.F. Zhong, T.B. Huang, J.M. Liu, G.H. Li, T.L. Lo, Y.G. Zhang, Z.L. Sun, S.M. Du, Q.Y. He, S.I. Wang, Economical deposition of a large area of high quality diamond film by a high power DC arc plasma jet operating in a gas recycling mode, *Diam. Relat. Mater.* 9 (2000) 1655–1659.
- [9] S. Noda, K. Hagiwara, O. Ichikawa, K. Tanabe, T. Yahiro, H. Ohkawa, T. Osawa, H. Komiyama, Closed recycle CVD process for mass production of SOG-Si from MG-Si, Photovoltaic Specialists Conference, Conference Record of the 19th IEEE, 2002, pp. 308–311.
- [10] M.E. Collingham, R.L. Zollars, Effect of recycling on the axial distribution of coating thickness in a low pressure CVD reactor, *J. Electrochem. Soc.* 136 (1989) 787–794.
- [11] K.F. Jensen, D.B. Graves, Modeling and analysis of low pressure CVD reactors, *J. Electrochem. Soc.* 130 (1983) 1950–1957.
- [12] F. Maury, L. Gueroudji, C. Vahlas, Selection of metalorganic precursors for MOCVD of metallurgical coatings: application to Cr-based coatings, *Surf. Coat. Technol.* 86–87 (1996) 316–324.
- [13] A.C. Jones, P. O'Brien, CVD of Compound Semiconductors, VCH, Weinheim, 1997.
- [14] T.T. Kodas, M.J. Hampden-Smith, *The Chemistry of Metal CVD*, VCH, Weinheim, 1994.
- [15] F. Maury, F. Ossola, Evaluation of tetra-alkylchromium precursors for OMCVD: I — films grown using  $\text{Cr}[\text{CH}_2\text{C}(\text{CH}_3)_3]_4$ , *Thin Solid Films* 207 (1992) 82–89.
- [16] S. Abisset, F. Maury, Low temperature MOCVD of V-C-N coatings using bis(arene) vanadium as precursors, *Surf. Coat. Technol.* 108–109 (1998) 200–205.
- [17] W. Hafner, E.O. Fischer, *British Patent 976 573*, Nov. 25, 1964.
- [18] N.G. Anantha, V.Y. Doo, D.K. Seto, Chromium deposition from dicumene-chromium to form metal-semiconductor devices, *J. Electrochem. Soc.* 118 (1971) 163–165.
- [19] F. Maury, D. Ouqab, J.C. Manse, R. Moranchio, J.F. Nowak, J.P. Gauthier, Structural characterization of chromium carbide coatings deposited at low temperature by LPCVD process using dicumene chromium, *Surf. Coat. Technol.* 41 (1990) 51–61.
- [20] F. Schuster, F. Maury, J.F. Nowak, Influence of organochromium precursor chemistry on the microstructure of MOCVD chromium carbide coatings, *Surf. Coat. Technol.* 43–44 (1990) 185–198.
- [21] V.B. Polikarpov, A.S. Luzin, V.A. Dodonov, E.K. Klement, Chromium films obtained by pyrolysis of chromium bisarene complexes in the presence of chlorinated hydrocarbons, *Izv. Akad. Nauk SSSR* 20 (1983) 1839–1842.
- [22] T.P. Whaley, V. Norman, Carbonaceous solid bodies and processes for their manufacture, *US Patent 3 252 824*, May 24, 1966.
- [23] F. Schuster, F. Maury, J.F. Nowak, C. Bernard, Characterization of chromium nitride and carbonitride coatings deposited at low temperature by OMCVD, *Surf. Coat. Technol.* 46 (1991) 275–288.
- [24] F. Maury, C. Vahlas, S. Abisset, L. Gueroudji, Low temperature MOCVD routes to chromium metal thin films using bis(benzene)chromium, *J. Electrochem. Soc.* 146 (1999) 3716–3723.
- [25] A.S. Luzin, V.B. Polikarpov, V.A. Dodonov, E.K. Klement, Chromium films produced by pyrolysis of its bis-arene complexes in the presence of sulfur-containing additives, *Zh. Prikl. Khim.* 61 (1988) 1235–1239.
- [26] F. Maury, A. Douard, S. Delclos, D. Samelot, C. Tendero, Multilayer chromium based coatings grown by atmospheric pressure direct liquid injection CVD, *Surf. Coat. Technol.* 204 (2009) 983–987.
- [27] T. Drozda, C. Wick, J.T. Benedict, R.F. Veilleux, R. Bakerjian, Tool and manufacturing engineers handbook, in: P.E. Mitchell (Ed.), *Plastic part manufacturing*, 4th edition, Society of Manufacturing, vol. 8, 1996.
- [28] B. Bryskin, A. Kostylev, Y. Pokrovskiy, A. Lumpov, Innovative processing technology of chromium carbide coating to apprise performance of piston rings, *SAE Int. J. Mater. Manuf.* 6 (2013) 131–134.
- [29] C. Vahlas, F. Maury, L. Gueroudji, A thermodynamic approach to the chemical vapor deposition of chromium and of chromium carbides starting from  $\text{Cr}(\text{C}_6\text{H}_6)_2$ , *Chem. Vap. Depos.* 4 (1998) 69–76.
- [30] A. Douard, C. Bernard, F. Maury, Thermodynamic simulation of Atmospheric DLI-CVD processes for the growth of chromium based hard coatings using bis(benzene) chromium as molecular source, *Surf. Coat. Technol.* 203 (2008) 516–520.
- [31] A. Michau, F. Maury, F. Schuster, R. Boichot, M. Pons, Chromium Carbide Growth by Direct Liquid Injection Chemical Vapor Deposition in Long and Narrow Tubes, Experiments, Modeling and Simulation (submitted for publication), (2017).
- [32] T.N. Blanton, D. Majumdar, Characterization of X-ray irradiated graphene oxide coatings using X-ray diffraction, X-ray photoelectron spectroscopy, and atomic force microscopy, *Powder Diffract.* 28 (2013) 68–71.
- [33] V.Q. Bui, H.M. Le, Y. Kawazoe, D. Nguyen-Manh, Graphene-Cr-Graphene intercalation nanostructures: stability and magnetic properties from density functional theory investigations, *J. Phys. Chem. C* 117 (2013) 3605–3614.
- [34] S. Sarkar, S. Niyyogi, E. Bekyarova, R.C. Haddon, Organometallic chemistry of extended periodic  $\pi$ -electron systems: hexahapto-chromium complexes of graphene and single-walled carbon nanotubes, *Chem. Sci.* 2 (2011) 1326–1333.
- [35] M.N. Iliiev, A.P. Litvinchuk, H.G. Lee, C.W. Chu, A. Barry, J.M.D. Coey, Raman spectroscopy of ferromagnetic  $\text{CrO}_2$ , *Phys. Rev. B* 60 (1999) 33–36.
- [36] T. Yu, Z.X. Shen, J. He, W.X. Sun, S.H. Tang, J.Y. Lin, Phase control of chromium oxide in selective microregions by laser annealing, *J. Appl. Phys.* 93 (2003) 3951–3953.
- [37] H.C. Barshilia, N. Selvakumar, K.S. Rajam, A. Biswas, Structure and optical properties of pulsed sputter deposited  $\text{Cr}_x\text{O}_y/\text{Cr}/\text{Cr}_2\text{O}_3$  solar selective coatings, *J. Appl. Phys.* 103 (2008) 023507.
- [38] A.C. Ferrari, J. Robertson, Raman spectroscopy of amorphous, nanostructured, diamond-like carbon, and nanodiamond, *Philos. Trans. R. Soc. Lond. A* 362 (2004) 2477–2512.
- [39] P.K. Chu, L. Li, Characterization of amorphous and nanocrystalline carbon films, *Mater. Chem. Phys.* 96 (2006) 253–277.
- [40] L.G. Caçado, A. Jorio, E.H.M. Ferreira, F. Stavale, C.A. Achete, R.B. Capaz, M.V.O. Moutinho, A. Lombardo, T.S. Kulmala, A.C. Ferrari, Quantifying defects in graphene via Raman spectroscopy at different excitation energies, *Nano Lett.* 11 (2011) 3190–3196.
- [41] V.D. Aleksandrov, Vapor-phase deposition of coatings from bis-arene chromium compounds on aluminum alloys, *Met. Sci. Heat Treat.* 44 (2002) 160–162.
- [42] V.I. Yurshev, R.I. Mukatdarov, I.V. Yurshev, Surface hardening of tools by depositing a pyrolytic chromium carbide coating, *Met. Sci. Heat Treat.* 57 (2015) 107–111.
- [43] Z. Zeng, L. Wang, A. Liang, J. Zhang, Tribological and electrochemical behavior of thick Cr-C alloy coatings electrodeposited in trivalent chromium bath as an alternative to conventional Cr coatings, *Electrochim. Acta* 52 (2006) 1366–1373.
- [44] V.S. Protsenko, F.I. Danilov, V.O. Gordienko, A.S. Baskevich, V.V. Artemchuk, Improving hardness and tribological characteristics of nanocrystalline Cr-C films obtained from Cr(III) plating bath using pulsed electrodeposition, *Int. J. Refract. Met. Hard Mater.* 31 (2012) 281–283.
- [45] G.A. Lausmann, Electrolytically deposited hardchrome, *Surf. Coat. Technol.* 86–87 (1996) 814–820.
- [46] A. Liang, L. Ni, Q. Liu, J. Zhang, Structure characterization and tribological properties of thick chromium coating electrodeposited from a Cr(III) electrolyte, *Surf. Coat. Technol.* 218 (2013) 23–29.
- [47] A. Aubert, J. Danroc, A. Gaucher, J.P. Terrat, Hard chrome and molybdenum coatings produced by physical vapour deposition, *Thin Solid Films* 126 (1985) 61–67.
- [48] G. Cholvy, J.L. Derep, M. Gantois, Characterization and wear resistance of coatings in the Cr-C-N ternary system deposited by physical vapour deposition, *Thin Solid Films* 126 (1985) 51–60.
- [49] D.Y. Wang, K.W. Weng, C.L. Chang, W.Y. Ho, Synthesis of  $\text{Cr}_3\text{C}_2$  coatings for tribological applications, *Surf. Coat. Technol.* 120–121 (1999) 622–628.
- [50] Y.L. Su, T.H. Liu, C.T. Su, T.P. Cho, Effect of chromium content on the dry machining performance of magnetron sputtered  $\text{Cr}_x\text{C}$  coatings, *Mater. Sci. Eng. A* 364 (2004) 188–197.
- [51] J. Esteve, J. Romero, M. Gómez, A. Lousa, Cathodic chromium carbide coatings for molding die applications, *Surf. Coat. Technol.* 188–189 (2004) 506–510.
- [52] J. Romero, E. Martinez, J. Esteve, A. Lousa, Nanometric chromium nitride/chromium carbide multilayers by R.F. magnetron sputtering, *Surf. Coat. Technol.* 180–181 (2004) 335–340.
- [53] B. Bryskin, A. Kostylev, Y. Pokrovskiy, A. Lumpov, CVD technology for preparing wear-resistant chromium carbide coatings of engine components, *SAE Int. J. Mater. Manuf.* 7 (2014) 630–632.
- [54] T.Y. Tsui, G.M. Pharr, W.C. Oliver, C.S. Bhatia, R.L. White, S. Anders, A. Anders, I.G. Brown, Nanoindentation and nanoscratching of hard carbon coatings for magnetic disks, *MRS Online Proceedings Library Archive*, 383 1995, pp. 447–452.
- [55] J. Musil, P. Karváňková, J. Kasl, Hard and superhard Zr–Ni–N nanocomposite films, *Surf. Coat. Technol.* 139 (2001) 101–109.
- [56] M. Nowak, F. Lofaj, P. Hviscova, The effect of residual stresses on nanoindentation behavior of thin W-C based coatings, *Powder Metall. Prog.* 13 (2013) 132–138.
- [57] B. Xiao, J. Feng, C.T. Zhou, Y.H. Jiang, R. Zhou, Mechanical properties and chemical bonding characteristics of  $\text{Cr}_7\text{C}_3$  type multicomponent carbides, *J. Appl. Phys.* 109 (2011) 023507.
- [58] C.A. Klein, How accurate are Stoney's equation and recent modifications, *J. Appl. Phys.* 88 (2000) 5487–5489.
- [59] S. Wu, Q. Guo, S. Wu, C. Zhao, Modified curvature method for residual thermal stress estimation in coatings, *Surf. Eng.* 20 (2014) 866–870.
- [60] E. Bauer-Grosse, Thermal stability and crystallization studies of amorphous TM-C films, *Thin Solid Films* 447–448 (2004) 311–315.
- [61] M. Magnuson, M. Andersson, J. Lu, L. Hultman, U. Jansson, Electronic structure and chemical bonding of amorphous chromium carbide thin films, *J. Phys. Condens. Matter* 24 (2012) 225004–225010.
- [62] N.N. Travkin, B.G. Gribov, V.P. Romyants, Thermal decomposition of bisarene compounds of chromium, *Zh. Obshch. Khim.* 40 (1970) 2677.
- [63] G.G. Devyatkykh, V.A. Umlin, Y.V. Zverev, I.A. Frolov, Composition of impurities in bis-ethylbenzene chromium produced according to the Friedel-Crafts method, *Bull. Acad. Sci. USSR Div. Chem. Sci.* 18 (1969) 207–209.
- [64] B.G. Gribov, Super-pure materials from metal-organic compounds, *Russ. Chem. Rev.* (translated from *Uspekhi Khimii*) 42 (1973) 893–903.
- [65] A. Douard, Dépôt de carbures, nitrures et multicouches nanostructurées à base de chrome sous pression atmosphérique par DLI-MOCVD: nouveaux procédés et potentialités de ces revêtements métallurgiques (PhD dissertation), INP Toulouse, 2006, <https://tel.archives-ouvertes.fr/tel.-00376437>.